Supplemental Information

FAK Regulates the Localization and Retention of Pro-B Cells in BM Microenvironments.

Shin-Young Park, Peter Wolfram, Kimberly Canty, Brendan Harley, César Nombela-Arrieta, Gregory Pivarnik, John Manis, Hilary E Beggs, and Leslie E Silberstein

Figure S1. Analysis of *Cre*-mediated *Fak* deletion. (A) Schematic representation of the wild type, floxed *Fak* allele, and excised locus. (B) PCR and immunoblot (IB) analysis of BM $CD19^{+}$ B cells (purity > 97%) and whole BM (WBM) from CD19-$Cre^{+/-}$ $Fak^{fl/fl}$ knock out mice (KO) and CD19-$Cre^{-/-}$$Fak^{fl/fl}$ control mice (WT; 8 week old). *Fak* gene assessed by PCR with primer 1, 2 and 3. FAK protein expression by WB with a monoclonal anti-FAK antibody (Upstate Biotech.) (C) *Fak* gene deletion by PCR in sorted B cells of BM: Pro-B ($CD19^{+}$ $B220^{lo}$ $CD43^{+}$ IgM^{-}), Pre-B ($CD19^{+}$ $B220^{lo}$ $CD43^{-}$ IgM^{-}), Immature B cells (Imm B, $CD19^{+}$ $B220^{lo}$ IgM^{+}), Mature B cells (Mat B, $CD19^{+}$ $B220^{hi}$ IgM^{+}) of *Fak* KO mice. (D) PCR and immunoblot analysis of splenic $CD19^{+}$ B cells of *Fak* KO and WT control mice. Representative data from four independent experiments are shown. (E) Immunoblot (IB) analysis of Pyk2 protein level with monoclonal anti-Pyk2 (Transduction Laboratory) antibodies in sorted B cells of BM: Pro-B, Pre-B, Immature B cells (Imm B), Mature B cells (Mat B) of WT and *Fak* KO mice. After secondary horseradish peroxidase-conjugated antibodies (Bio-Rad) were treated, immunoblots were analyzed by enhanced chemiluminescence (Amersham Biosciences). (F) *Cre*-mediated excision of floxed stop codon leads to EGFP gene expression. PCR analysis of *Cre*-mediated *Fak* gene deletion were performed with primer P1, P2, and P3 in $EGFP^{+}$ cells (G2 gate) and $EGFP^{-}$ control cells (G1 gate) of CD19-$Cre^{+/-}$ $Fak^{fl/fl}$ ROSA26-$EGFP^{+}$ (KO) mice. ROSA26-$EGFP^{-}$ mice were used as controls for flow cytometry. (G) *Fak* gene deletion was analyzed by PCR in sorted B cell subpopulations from mb-1-$Cre^{+/-}$ $Fak^{fl/fl}$ ROSA26-$EGFP^{+}$ or mb-1-$Cre^{+/-}$ $Fak^{wt/wt}$ ROSA26-$EGFP^{+}$ mice. BM $CD3^{+}$ T cell from mb-1-$Cre^{+/-}$

$Fak^{fl/fl}$ ROSA26-EGFP^{+} mice and BM CD19^{+} B cells from control WT mice were used as controls. (H) *Cre*-mediated excision of floxed genes were monitored by EGFP gene expression in B cell populations of mb-1-$Cre^{+/-}$ $Fak^{fl/fl}$ ROSA26-EGFP^{+} mice. B220^{-} cells were used as negative controls. % of EGFP^{+} cell population is marked above each gate. Representative data from four independent experiments are shown.

Figure S2. ***Fak* deletion does not affect the number of follicular and marginal zone B cells in spleen.** (A) Single cell suspensions from spleen were analyzed by flow cytometry. Gate: Imm – CD19^{+} CD23^{-} CD21/35^{-} immature B cells, FO – CD19^{+} CD23^{+} CD21/35^{mid} follicular B cells, MZ – CD19^{+} CD23$^{-/lo}$ CD21/35^{hi} marginal zone B cells. (B) Splenic transitional B cells were analyzed by flow cytometry. IgM^{+} CD23^{-} transitional 1 (T1), IgM^{+} CD23^{+} transitional 2 (T2), and IgM^{-} CD23^{+} transitional 3 (T3) B cells were gated as shown. % of gated cell population is marked next to each gate. Representative data from four independent experiments are shown. (C) Total numbers of each transitional B subset cells per spleen were calculated using flow cytometry. Student's t-tests were performed as shown *, $P<0.05$ and **, $P<0.01$ (Unpaired, two-tailed).

Figure S3. **Laser scanning cytometry analysis of spleen sections and morphology of the femoral BM cavity.** (A) Validation of quantitative imaging cytometry on 5μm histologic sections of cryopreserved splenic tissue. B220^{+} B cells (green) and nucleated cells (blue, DAPI) in C57BL/6 mouse spleen. Image: laser scan mosaic image of the entire tissue section. Scale bar: 500μm. Frozen sections were stained with rat anti-B220 antibody (RA3-6B2, BD Biosciences) or isotype control antibody (rat IgG2a, BD Biosciences) followed by Alexa 488- labeled secondary antibody and DAPI nuclear staining dye. Individual cellular events are identified by nuclear staining (DAPI). % of B220+ cells were gated from dot plot. (B) Hematoxylin and Eosin (H&E) staining of the femoral bone from C57BL/6 wild type

mouse. The magnified diaphyseal cavity shows cortical bone surrounding dense BM and a portion of central sinus (pink cavity). The distal metaphysis shows the characteristic trabecular bone structure with BM within the trabeculae. Blue arrows: bone surface, Black dotted region: endosteal region, Black arrows: vascular system, Green dotted region: central medullary region. Representative data from four independent experiments are shown.

Figure S4. **Localization of progenitor B cells in femoral BM microenvironments by solid-phase laser scanning cytometry.** Longitudinal femur sections from C57BL/6 wild type (WT) mice were stained with B cell markers. Sinusoidal niche was stained by goat anti-CD105 (endoglin) antibody / Dylight 649-labeled donkey anti-goat IgG antibody (white), followed by nuclear DAPI staining (blue). Stained slides were analyzed by iCys imaging cytometry. (A) A square area of a femur is magnified to show a representative region image. (B) Representative field images of CD43, B220, and endoglin /DAPI channels are shown. Arrowheads indicate B220^{+} CD43^{+} pro-B cell. (C) A field image of DAPI channel is shown with threshold contours which are expanded by 2 pixels for integration contours. (D) Fluorescence intensity in different channels is quantified for each individual event as shown in a dot plot with specific gates based on isotype control staining. Numbers within the plot indicate the percentage of cells in each population. Representative data from four independent experiments are shown.

Park et al., Figure S1

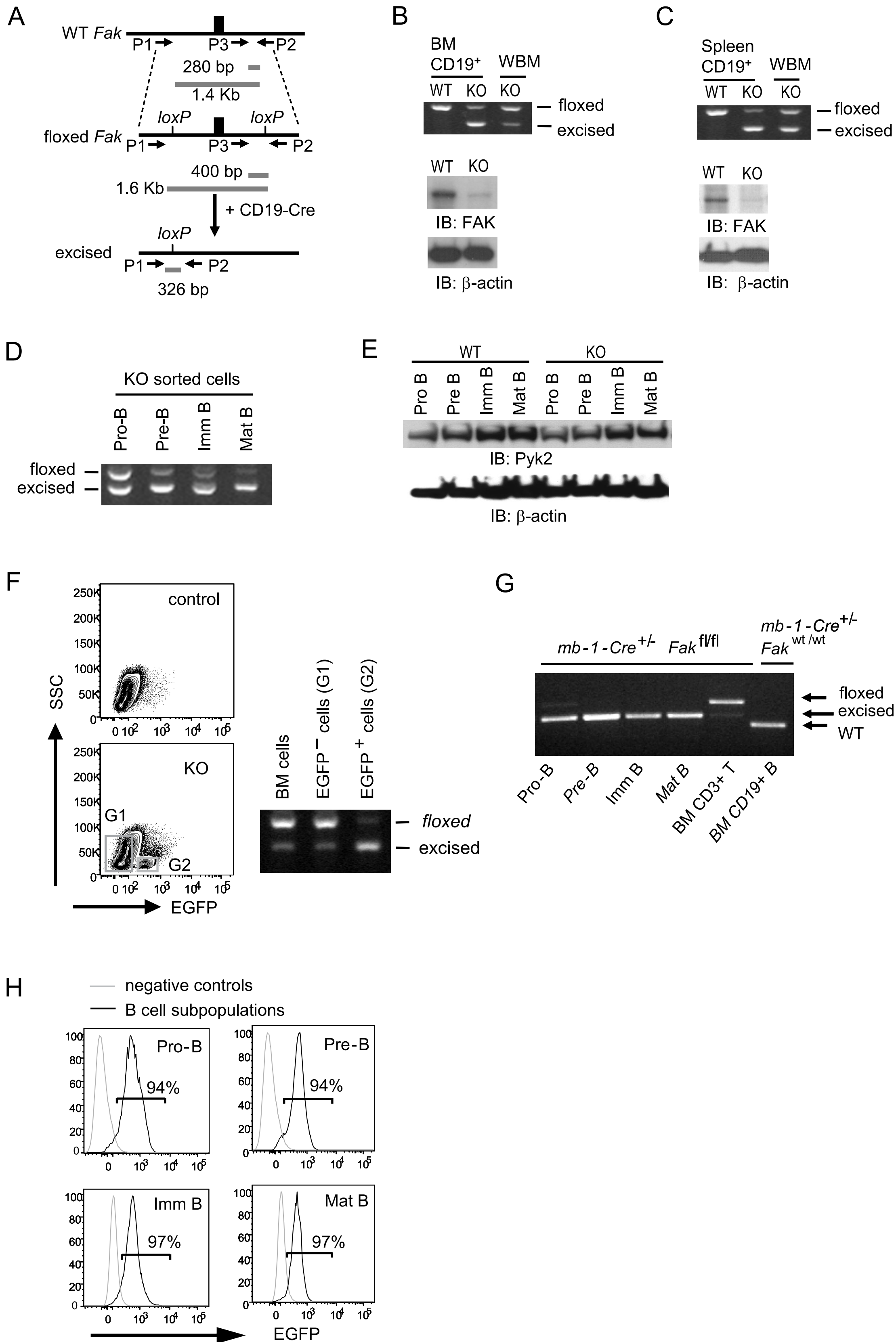

Park et al., Figure S2

A

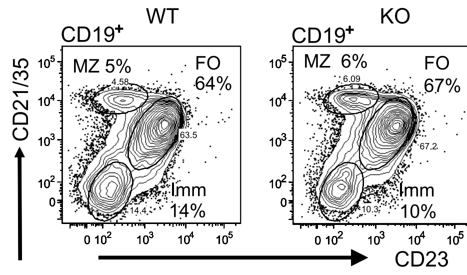

B

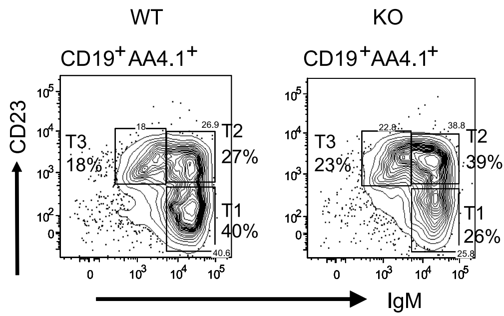

C

Number of transitional B cells in spleen

Subset	WT	KO
T1	2.39 ± 0.15	1.65 ± 0.17**
T2	1.82 ± 0.13	2.31 ± 0.14*
T3	1.17 ± 0.08	1.38 ± 0.10

(mean ± SEM, millions, n=8)

Park et al., Figure S3

A

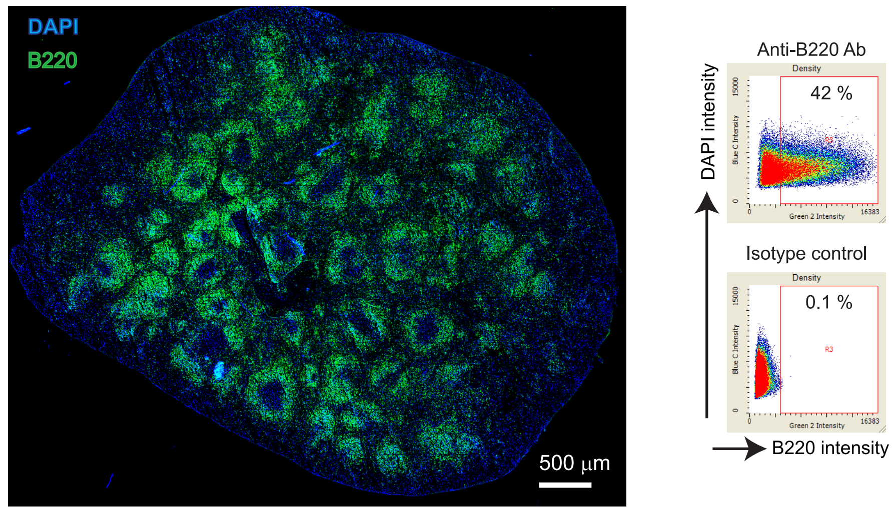

B

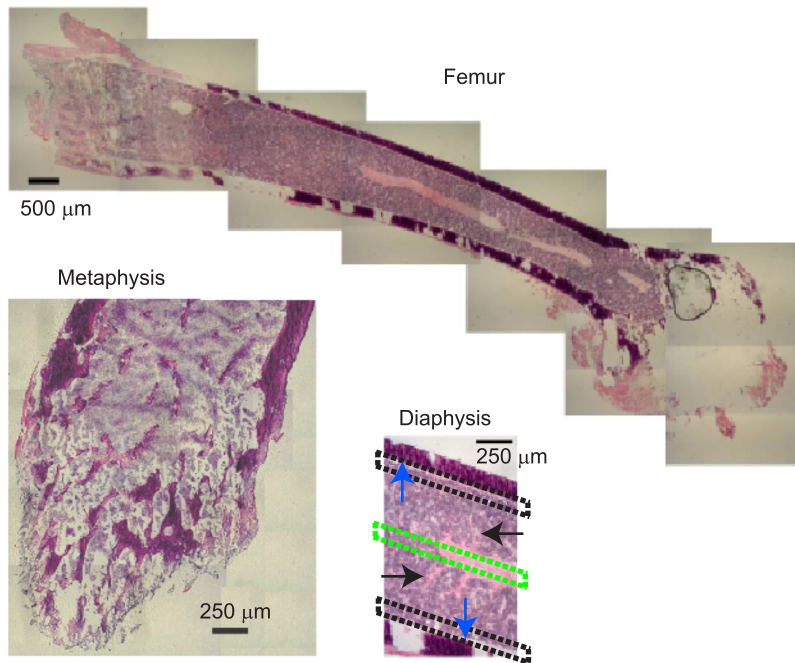

Park et al., Figure S4